2011-06-28

Magnetic Field Sensing with Slab Coupled Optical Fiber Sensors

Bryson J. Shreeve
Brigham Young University - Provo

Magnetic Field Sensing with Slab Coupled Optical Fiber Sensors

Bryson Shreeve

A thesis submitted to the faculty of
Brigham Young University
in partial fulfillment of the requirements for the degree of

Master of Science

Stephen M. Schultz, Chair
Richard H. Selfridge
Gregory P. Nordin

Department of Electrical and Computer Engineering

Brigham Young University

August 2011

ABSTRACT

Magnetic Field Sensing with Slab Coupled Optical Fiber Sensors

Bryson Shreeve
Department of Electrical and Computer Engineering, BYU
Master of Science

This thesis reports an in-fiber magnetic field sensor that is able to detect magnetic fields as low as 2 A/m at a spatial resolution of 1 mm. The small sensor consists of a magneto-optic slab waveguide, bismuth-doped rare earth iron garnet (Bi-RIG) that is coupled to an optical fiber. By coupling light from the fiber to the slab waveguide, it becomes an in-fiber magnetic field sensor. This is due to the Magneto-Optic Kerr effect; a change in refractive index is proportional to the applied magnetic field. When an AC field is applied, an AC component in the output power can be detected by a spectrum analyzer.

The novelties of Magneto-Optic Slab Coupled Optical Sensor (MO-SCOS) devices include their small compact nature and a dielectric structure allowing low electromagnetic interference. Due to their compact size they are capable of placement within devices to measure interior electromagnetic fields immeasurable by other sensors that are either too large for internal placement or disruptive of the internal fields due to metallic structure.

This work also reports progress on EO SCOS development. The EO sensor has found application in new environments including the electromagnetic rail gun, and a dual-axis sensor.

Keywords: Bryson Shreeve, magnetic field sensor, electric field sensor, optics, fiber optics, optical fiber sensor, d-fiber

ACKNOWLEDGMENTS

First and foremost, I would like to thank my wife for all of her support and patience during my work in graduate school. She has been an inspiration to me. I thank all my family for their support as well, especially my mother who always encourages further education.

I would also like to thank my advisors, Dr. Selfridge and Dr. Schultz. Their guidance and novel ideas helped me to gain a love for optics. I thank them for their time spent mentoring me through school, research, and writing. I am also grateful for all the help I have received from my peers. I am especially thankful for my mentor Richard Gibson, whose work in electro-optic sensors provided the foundation from which my magneto-optic sensor was based. I also thank all of the students in the Optics lab, their ideas and suggestions have helped me often in my research.

My research would not have been possible without the support of our funders including IPITEK who has invested both time and money in my projects and KVH who has donated the D-fiber used extensively throughout the lab. I also thank my university, Brigham Young University, and especially the Electrical Engineering department which values student development more than all else.

TABLE OF CONTENTS

LIST OF FIGURES

1 INTRODUCTION

In-fiber devices are useful in a variety of applications due to their small size and low insertion loss. One class of in-fiber devices utilizes the Slab Coupled Fiber (SCF) technique. The SCF technique uses resonant coupling between an optical fiber and a slab waveguide to create an in-fiber device. Devices made with this technique include polarizers [1], filters [2], and sensors [3-5]. A branch of the SCF devices uses a D-shaped fiber as the platform. These Slab Coupled Optical Sensor (SCOS) devices depend on mode coupling to transition optical power from the fiber to the slab waveguide on the flat side of the D-fiber. A primary technology that utilizes the SCOS technique is the Electro-optic sensor [6].

A magnetic field sensor has now been developed using the D-fiber slab coupled sensor technique. The device combines a magneto-optic slab waveguide with a D-fiber to measure magnetic fields. This so-called Magneto-Optic Slab Coupled Optical Sensor (MO-SCOS) is shown to measure magnetic fields as low as 2 A/m. Because of its small interaction length, the sensor can map fields with a spatial resolution as low as 1 mm.

1.1 The Need for Optical Fiber Based Magnetic Field Sensors

One important application for magnetic field sensing is safeguarding electronics. High powered microwave (HPM) and electromagnetic pulse (EMP) weapons pose severe concerns on the safety and reliability of electronic equipment [7-10]. These weapons are engineered to

generate short, high-powered, high-frequency pulses capable of coupling with conductive lines in electronics and inducing large transient currents to destroy sensitive circuitry and semiconductor devices. An attack from such weapons can quickly disable communications systems, databases, control systems, guidance systems, etc. and reduce a targeted military or civic region of all modern electronic equipment and technologies.

In order to protect electronics from HPM and EMP weapons, metallic shielding has been developed. To better understand the effectiveness of HPM and EMP weapons on shielded electronic circuitry, sensors are needed to measure high-frequency, high-energy pulses in close proximity to the circuitry within the shielding without affecting the electronics, the shielding, or significantly altering the fields within the target. Small electric field sensors have already been developed that could be placed within the metallic shielding to measure the electric fields [6]. This electric field sensor can determine how much of the field penetrates into the shielding. The electric field inside the shielding is not the end goal however; the current induced in the electronic circuitry is what will actually destroy the electronics. A magnetic field sensor can determine the current in a wire by measuring the accompanying magnetic field around the wire.

In order for a sensor to meet the requirements for measuring magnetic fields within shielding it must be made of dielectric materials. A sensor in this application must also be a small, flexible device that can be threaded within electronic components and circuitry. A sensor would also need to have a good resolution in order to spatially localize the magnetic fields. Many high precision magnetic field sensors are currently available, but most, like the magnetic field probe shown below in Figure 1-1 are made with electrical components. Although this B&K sensor [11], the B-dot sensor [12], and the Hall effect sensor [13] can measure weak magnetic fields often at high spatial resolution, they are susceptible to the HPM and EMP weapons that

need to be quantified in this application. Free space optical sensors, like a Faraday rotator [14] can be completely dielectric, but require a clear, straight path through the field. Newer Faraday rotators have been packaged to be in-fiber devices [15, 16] to avoid this limitation. Although these devices have small entry and exit requirements, the sensors themselves are still large. A smaller magnetic field sensor utilizes highly-terbium doped fiber [17]. This small, in-fiber device could easily fit the size requirements of the EMP shielding application, but has poor spatial resolution (the sensing region of this device is 2 cm long).

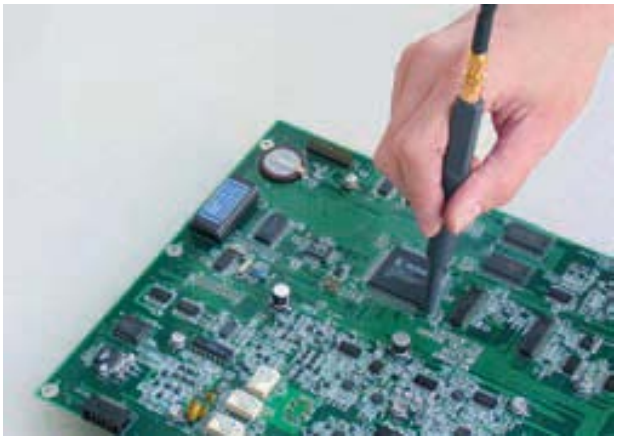

Figure 1-1: B&K PR 26M magnetic field probe.

SCOS technology satisfies all the requirements imposed by the HPM shielding application. A SCOS sensor is shown below in Figure 1-2 on a finger tip. It is completely dielectric, has a good spatial resolution, and can be placed anywhere that is accessible by an optical fiber. Furthermore, this fiber-based solution could allow for sensor multiplexing in order to map multiple instances of a field within the device under test [18].

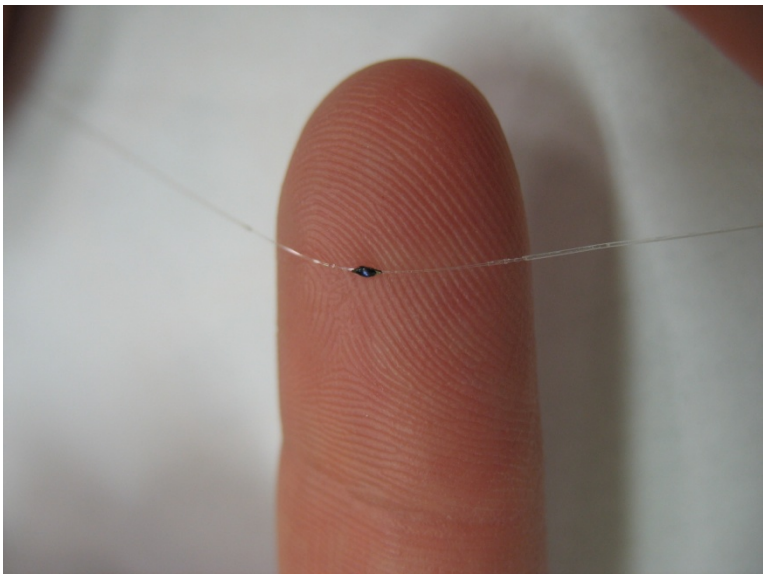

Figure 1-2: MO SCOS sensor on a finger tip. The crystal itself is about 1mm x 0.5 mm x 0.2 mm.

1.2 Contributions

The main contribution of this work has been the development of an all dielectric magnetic field sensor with a spatially localized field measurement. This contribution is divided into the following parts.

- I designed a magneto-optic sensor based on coupling of light between a D-fiber and a slab of Bi-RIG (a magneto-optic material). The technique is called MO-SCOS.
- I developed the techniques to fabricate the MO-SCOS.
- I characterized the MO-SCOS performance in terms of:
    - Signal strength
    - Field sensitivity
    - Spatial localization

The work on the MO-SCOS has been published in the following:

1. B. Shreeve, R. Selfridge, S. Schultz, A. Pulsipher, C. Gaeta, R. Forber, "D-fiber coupled Bi-RIG slab as a Magnetic field sensor," *To be Submitted*

2. B. Shreeve, R. Selfridge, S. Schultz, C. Gaeta, R. Forber, "Magnetic Field Sensor with Bi-RIG Slab Waveguide Coupled to D-type Optical Fiber," OFS, Ottawa, Ontario, Canada, May 2011

In addition to the development of the MO-SCOS technology, I have also had other less significant contributions as listed below.

- I integrated Electro-optic sensors into an electromagnetic rail gun.

- I have been involved in EO sensor research with several of my peers, including the multi-dimensional EO sensor.

The work on the application of the electro-optic SCOS has been published in the following:

1. B. Shreeve, R. Gibson, D. Perry, R. Selfridge, S. Schultz, R. Forber, W. Wang, J. Luo, "Non-intrusive Field Characterization in Interior Cavities with Slab Coupled Optical Sensor (SCOS)," *To be Published*

2. B. Shreeve, R. Gibson, D. Perry, R. Selfridge, S. Schultz, R. Forber, W. Wang, J. Luo, "Non-intrusive Field Characterization in Interior Cavities with Slab Coupled Optical Sensor (SCOS)," DEPS Conference, Albuquerque, NM, August 2010

1.3 Thesis Outline

Chapter 2 includes the background of SCOS devices, including mode coupling and fabrication. An analysis of the magneto-optic slab waveguides used in SCOS for magnetic field measurement is included in Chapter 3. In Chapter 4 the MO SCOS is used to measure magnetic fields. The minimum detectable field for a MO SCOS is determined. The sensor is also used to map the magnetic fields around long wires to demonstrate spatial sensitivity. Chapter 5 outlines

the work done in of the EO sensor area. An appendix is also included with the H-field MATLAB simulation code utilized in Section 4.4.

2 BACKGROUND

The SCOS works as an optical modulator to detect changes to refractive index. The SCOS consists of a multi-mode slab waveguide and a D-shaped optical fiber. Through mode coupling, the slab waveguide interacts with the optical power in the fiber. By choosing a slab whose index of refraction is dependent on an external factor, the power transmitted through the fiber becomes modulated by that same external factor. This chapter explains mode coupling and SCOS fabrication.

2.1 SCOS Operation

If two optical waveguides are in close enough proximity to each other that their evanescent fields overlap, light in one waveguide may couple into the guiding structure of the other waveguide. This chapter assumes SCOS operation based on the weak coupling condition. A more complete study of mode coupling, and why weak coupling can be assumed, has been done by Gibson [6]. In this weak coupling regime, resonances are analyzed by the eigenvalue equation for the slab waveguide modes, assuming phase matching with the fiber mode which remains unchanged across the wavelength range of the SCOS transmission spectrum [19].

Figure 2-1 shows that the basic SCOS device consists of a magneto-optic (MO) slab waveguide of thickness, *t*, in close proximity to the core of an optical fiber. Resonant mode coupling between the slab waveguide and D-shaped optical fiber (KVH Industries, Inc.) form the

basis for SCOS sensing. Full resonant transfer of optical power takes place for slab modes at wavelengths where the slab mode index equals the mode index of the fiber (assuming there is adequate evanescent overlap).

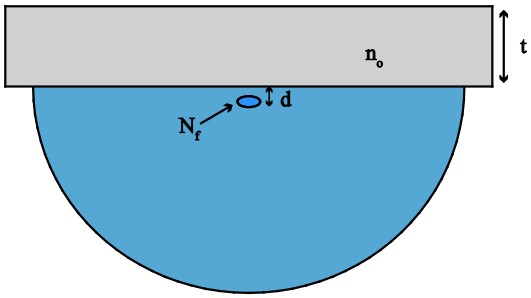

Figure 2-1: **Cross section diagram of the SCOS sensor**

The transmission spectrum of a SCOS consists of a periodic set of transmission dips corresponding to wavelengths where the light is resonantly coupled from the optical fiber to a mode in the multi-mode slab waveguide. Figure 2-2 shows a SCOS where modes coupled from the fiber are dispersed in the slab waveguide and the corresponding resonant dips are seen in the transmission spectrum.

As mentioned earlier, these resonant modes occur at wavelengths where the effective index of the fiber mode matches one of the modes in the slab waveguide. For a thick slab at higher order modes, the effective index of the m^{th} slab mode matches that of the fiber when the wavelength is given by [19]

$$\lambda_m = \frac{2t}{m}\sqrt{n_o^2 - N_f^2}\,, \tag{2-1}$$

where t and n_o are respectively the thickness and refractive index of the overlay material, N_f is the mode index of the fiber (1.451 for D-fiber at λ = 1550 nm), and m is the mode number.

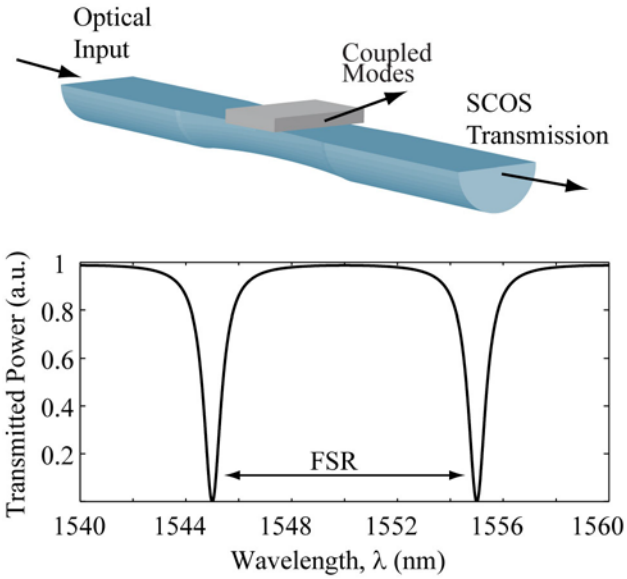

Figure 2-2: SCOS showing optical input into the D-fiber and a coupled slab waveguide where modes are scattered (Top). SCOS transmission from D-fiber output shows resonant modes (Bottom). The free spectral range (FSR) is the spacing between subsequent modes.

When an external factor changes the refractive index of the slab, the spectral position of the transmission dips also shifts. Detecting high frequency change in n_o requires monitoring the corresponding changes in transmitted power at a mid-resonant wavelength. This involves probing at a mid-resonant wavelength where the coupling slope is large as shown in Figure 2-3. When a change in n_o causes a shift of $\Delta\lambda$ in the transmission spectrum, the output at a mid-resonant wavelength is modulated by ΔT.

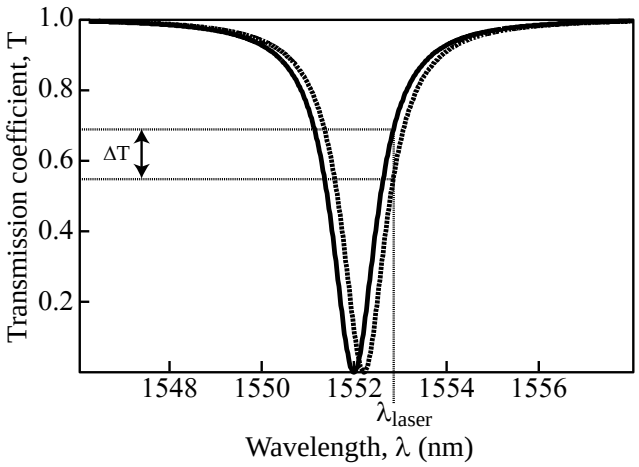

Figure 2-3: A small shift in wavelength generates an appreciable change in the transmission output for a SCOS sensor.

SCOS technology takes advantage of the highly sensitive nature of mode coupling in order to monitor small index changes in the slab material. By using a magneto-optic slab, the correlation between magnetic field strength and slab index makes the SCOS an effective magnetic field sensor. This correlation is based on the magneto-optic Kerr effect, and is discussed in Section 3.1. It is also important to note that the slab index varies with other factors including temperature, pressure and strain [20]. As appropriate, these environmental variables should be taken into consideration wherever a SCOS is used.

2.2 SCOS Fabrication

The geometry of the D-fiber provides a convenient platform for fabricating devices that involve mode coupling. Figure 2-4 shows that the fiber's elliptical core resides in close proximity to the flat surface of the D-fiber. Only a small portion of the cladding needs to be

removed in order to expose the evanescent portion of the fiber mode, leaving the fiber structurally sound and without significantly decreasing its mechanical strength.

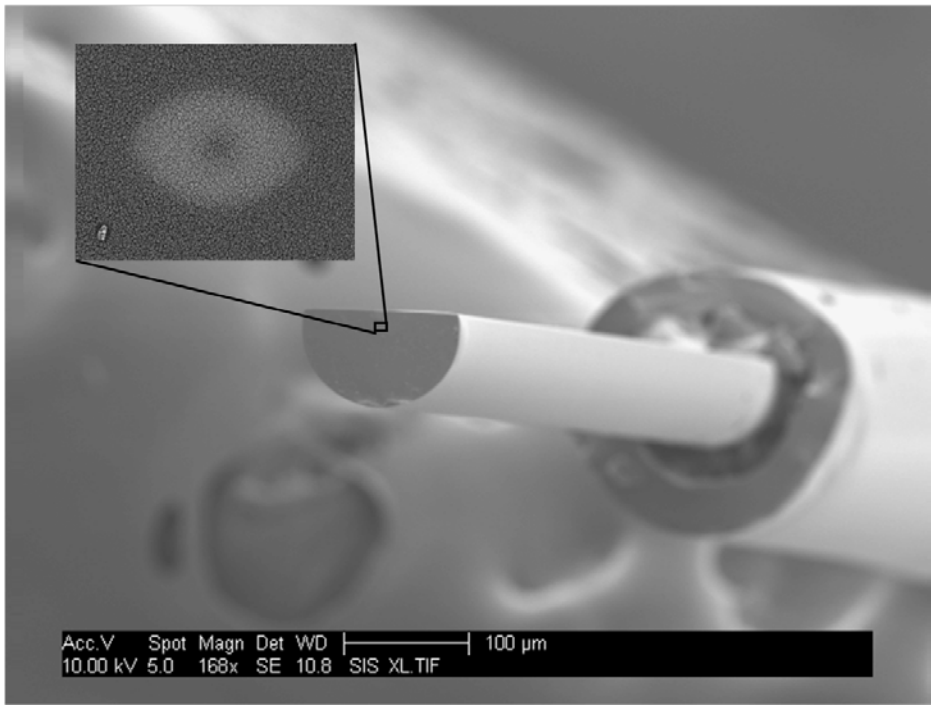

Figure 2-4: A 125 µm D-fiber with a 2 µm x 4 µm elliptical core located 13 µm from the flat surface.

Figure 2-5 shows the fabrication for SCOS devices in three main steps. (1) The D-fiber is thoroughly cleaned in preparation for wet etching. (2) The fiber is placed in a bath of hydrofluoric acid to etch down the cladding layer above the core. (3) A slab waveguide is coupled to the etched section of the D-fiber with an index matching adhesive. The hydrofluoric acid etching process enables full control over the evanescent coupling length and the corresponding coupling strength between fiber and slab waveguide [21]. Individual control over both the coupling length and strength are unique to the SCOS. A full description and analysis of

the etching process is not included here. This has been done previously [6]. This work will, however, explain the third step in SCOS fabrication, the slab placement.

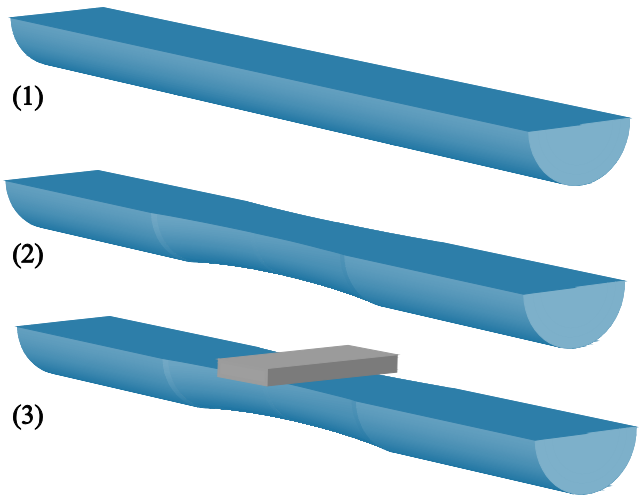

Figure 2-5: The SCOS fabrication process follows three steps 1) cleaning a stripped section of D-fiber, 2) hydrofluoric acid etching to expose evanescent fields, and 3) slab waveguide application for coupling to D-fiber.

The placement of the slab can be monitored in real time by using a broadband amplified stimulated emission source (ASE) as the input and an Optical Spectrum Analyzer (OSA) as the output as demonstrated in Figure 2-6. This in-situ monitoring is used to observe the expected mode resonances between fiber and slab to ensure proper placement, separation and positioning before permanent attachment. Figure 2-7 shows an example OSA screen capture before and after slab placement. Monitoring the placement allows manipulation of the coupling parameters of interaction length and core to slab distance (see Figure 2-8). The slab can be rotated to increase or decrease the transition region. More or less epoxy can also be used to increase or decrease the core to slab distance. The adhesive is ready for curing when the OSA shows deep,

low-loss resonances with narrow linewidths being transmitted through the SCOS. For a Bi-RIG slab, 10 dB from max to min is considered to be deep.

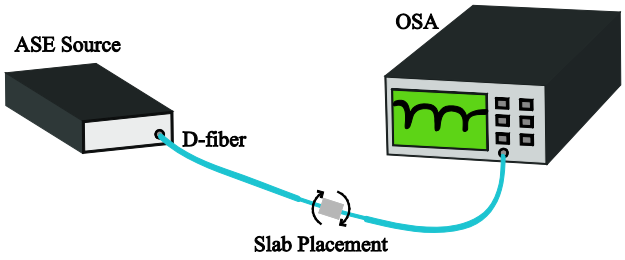

Figure 2-6: SCOS transmission is monitored using a broadband source and OSA as the correct slab placement is determined.

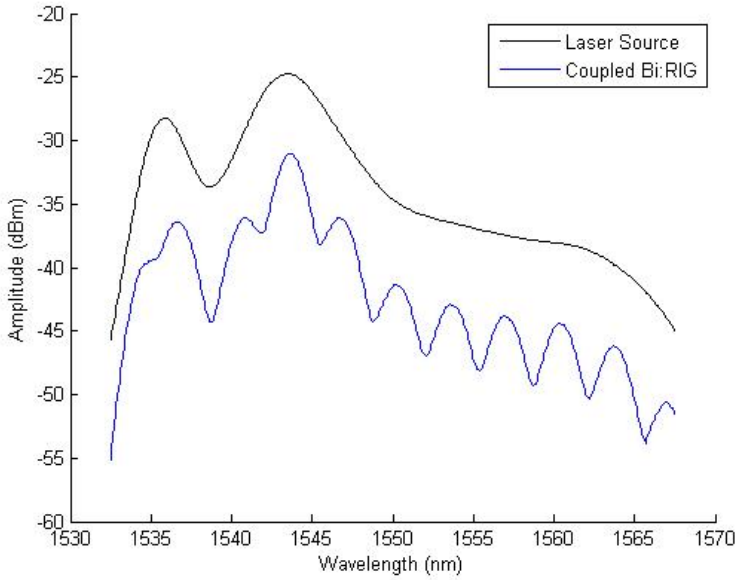

Figure 2-7: Sample OSA capture during slab placement. The broadband source before coupling is shown on top while the bottom shows the transmitted power after the MO slab has coupled.

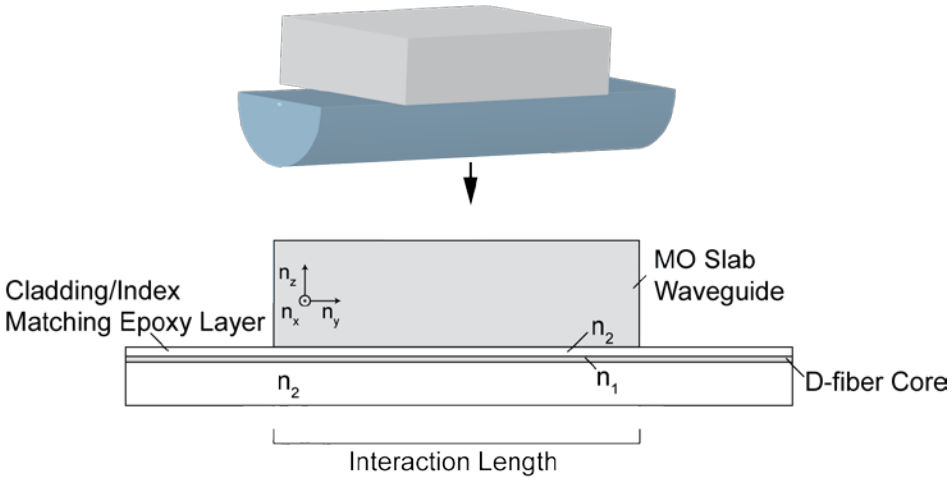

Figure 2-8: In-situ coupling allows for variation in interaction length and core to slab distance.

3 MAGNETO-OPTIC SLAB WAVEGUIDE

Using a MO material for the slab waveguide allows the SCOS to operate as a magnetic field sensor. The incident magnetic field changes the refractive index, n_o, of the slab, which in turn modulates the output power.

3.1 The Magneto-optic Effect

For a coupled waveguide to work as a magnetic field sensor, it must experience a change in refractive index as a function of applied field. The magneto-optic Kerr effect helps quantify the change of index with magnetic field, $\boldsymbol{H}$. The Kerr effect shows that gyrotropic materials can be classified by their gyration vector [22],

$$\boldsymbol{g} = \varepsilon_0 \chi^{(m)} \boldsymbol{H}, \tag{3-1}$$

where $\chi^{(m)}$ is the magneto-optical susceptibility. If $\boldsymbol{g}$ **(**and therefore $\boldsymbol{H}$**)** are in the z direction, the permittivity tensor in the simplest form becomes

$$\varepsilon = \begin{pmatrix} \varepsilon_1 & +jg_z & 0 \\ -jg_z & \varepsilon_1 & 0 \\ 0 & 0 & \varepsilon_2 \end{pmatrix}, \tag{3-2}$$

where ε_1 and ε_2 are attributes of the material. The off-diagonal terms containing g_z are sensitive to a magnetic field if the material is diamagnetic or paramagnetic. It can then be written

$$g_z = f\ H_z, \tag{3-3}$$

where f is related to the Verdet constant, *V*, as follows and H_z is the applied magnetic field. The *f* can be solved with

$$f = \frac{\lambda n V}{\pi}, \tag{3-4}$$

where *n* is the index of refraction of the material. In the ideal case, if one could take full advantage of the proper modal index changes in the slab created by a magnetic field the index change created by a field could be expressed as

$$\Delta n = \frac{\lambda V H}{\pi}. \tag{3-5}$$

This change in index would cause a shift in the wavelength in Equation (2-1). A larger Verdet constant will create a larger shift.

The Verdet constants of many MO materials are known at infrared wavelengths. The largest published is that of Terbium Gallium Garnet (TGG) [23]. Another MO material, Bismuth-doped rare earth iron garnet or Bi-RIG is also investigated. Although its Verdet constant is unpublished, its large Faraday rotation makes it a likely candidate to have a large *V*. The relationship between *V* and Faraday rotation is used to calculate the *V* for Bi-RIG at 1550 nm. *V* is directly related to Faraday rotation, β, by the following:

$$\beta = V \mu H d, \tag{3-6}$$

where μ is the permeability ($\mu = \mu_r \mu_o$), and d is the thickness. The relative permeability, μ_r, of the Bi-RIG sample [24] is about 1.2. To measure the Faraday rotation of the sample, a 500 µm thick piece is tested as shown in Figure 3-1; it is between an inductor pair with an on-axis separation distance approximately equal to the radius of the coil winding (Helmholtz coil format) and connected in series electrically. This configuration provides for optimum uniformity of the magnetic field at the midpoint of the separation while maintaining less than 6% variation elsewhere within the gap between the inductor pair. A polarizer/analyzer pair is employed to convert polarization rotation to variation in detected optical intensity. The magnetic field, *H*, in the gap of a Helmholtz coil is

$$H = \left(\frac{4}{5}\right)^{3/2} \frac{nI}{R}, \tag{3-7}$$

where *I* is the current, *R* is the radius of the inductor coil, and *n* represents the number of turns in each inductor. The measured rotation angle, θ, versus field, *H*, is shown in Figure 3-2. Using the values measured, the Faraday rotation is about 0.05 degrees/Oersted. Solving Equation (3-6) for *V* (where d = 500 µm and μ_r = 1.2) yields a Verdet constant of 16000 rad/T*m. This is 400 times larger than the Verdet constant of TGG.

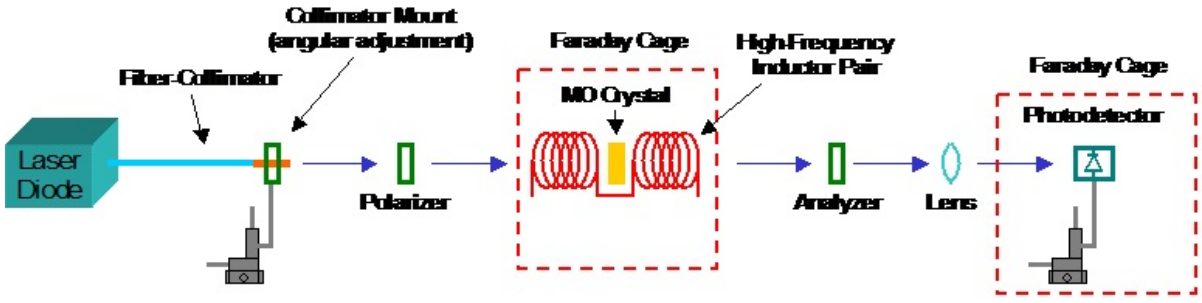

Figure 3-1: Experimental setup to determine Verdet constant of Bi-RIG.

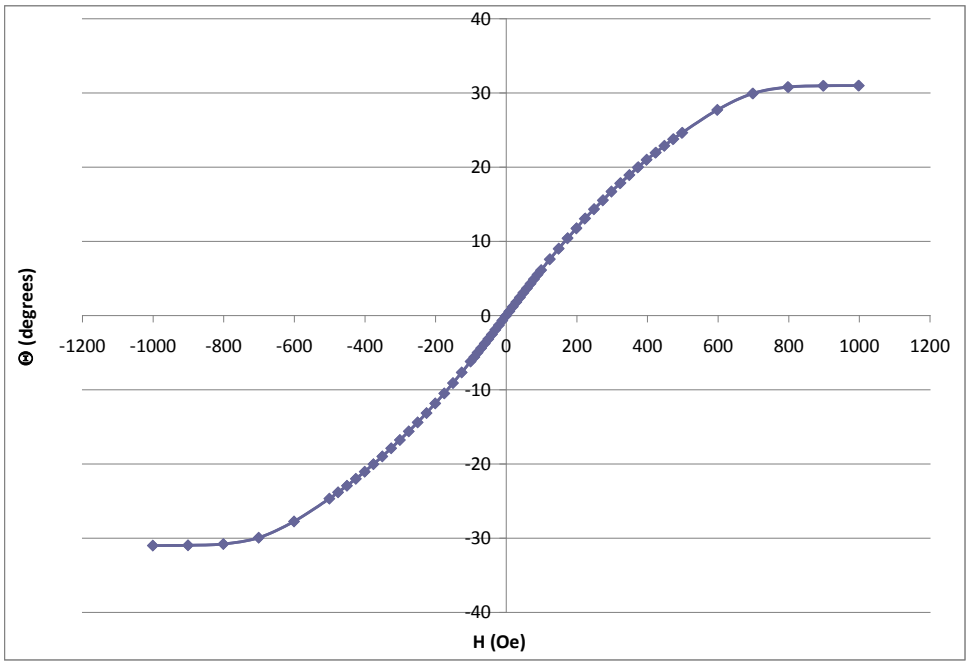

Figure 3-2: Measured Faraday rotation versus applied field.

3.2 The Fabricated MO SCOS

Figure 1-2 shows a fabricated SCOS sensor with a MO crystal. The crystal (which is bismuth-doped rare earth iron garnet, or Bi-RIG) is 0.2 mm thick and about 1 mm long by 0.5 mm wide. The normalized optical transmission for a particular MO sensor is displayed in Figure 3-3. The resonant dips are about 10 dB with free spectral range (FSR) of about 3 nm.

In the final product, the MO SCOS is often placed in protective packaging and either connectorized or fusion spliced with a standard fiber type to allow integration with systems using common fiber types. Packaging not only provides protection for the SCOS from breaking, but also isolates it from contamination. Figure 3-4 shows a typical packaged sensor. The fiber is secured with its flat side up by gluing it into a 50 mm long section of epoxy-glass. A strip in the center of the epoxy-glass substrate has been milled out to fit the fiber inside, while low index

epoxy secures it in place. The epoxy-glass, the same material used in many printed circuit boards, is used because it is rigid and non-conductive.

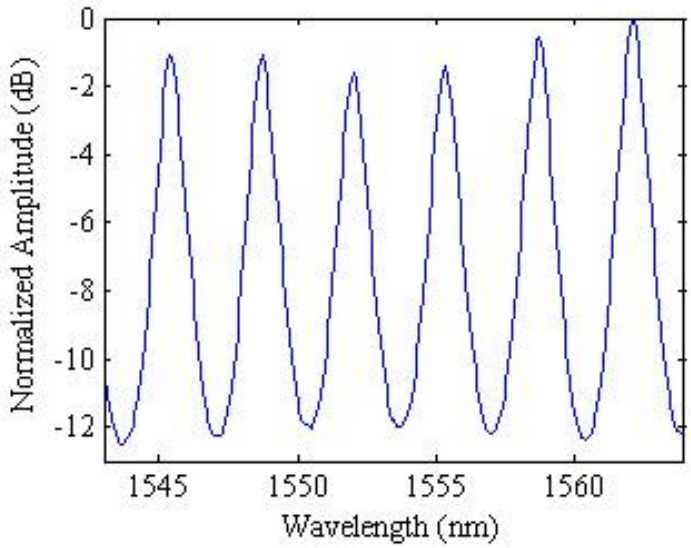

Figure 3-3: SCOS transmission for an EO polymer SCOS

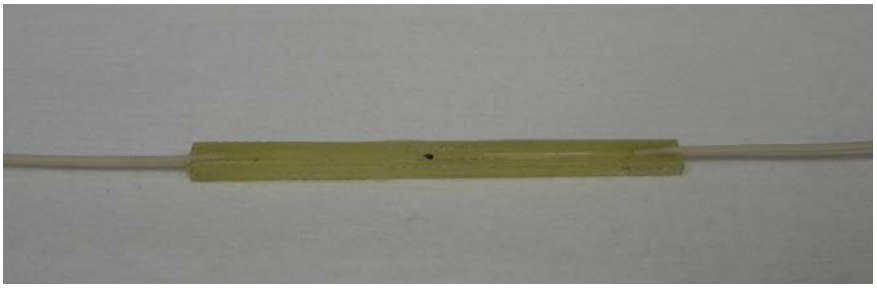

Figure 3-4: A packaged sensor. The black crystal (MO) is secured atop the fiber in the center of the rigid substrate. The substrate is typically about 50 mm x 6 mm x 2 mm.

Packaging can also provide a convenient way to designate SCOS orientation. Sensors that are highly orientation specific use this repeatable packaging method to keep the field-sensitive optic axis consistently normal to the top surface of the substrate.

4 MAGNETIC FIELD MEASUREMENTS

This chapter demonstrates the measurement capabilities of the Magneto-optic SCOS device. The minimum detectable field and the spatial resolution are determined using a known magnetic field created by a long current-bearing wire. This chapter begins by explaining the long wire experimental setup. Next, the MO-SCOS signal measurement technique is illustrated. Then, using the long wire and SCOS signal measurement setup, the minimum detectable field is shown to be 2 A/m. The spatial resolution of the sensor is then determined to be 1 mm.

4.1 Experimental Setup

The source of the magnetic field in the following experiments is a long current carrying wire. The magnetic field follows the pattern shown in Figure 4-1. For most of the experiments, a single wire creates the field of interest. One experiment however utilizes two parallel wires.

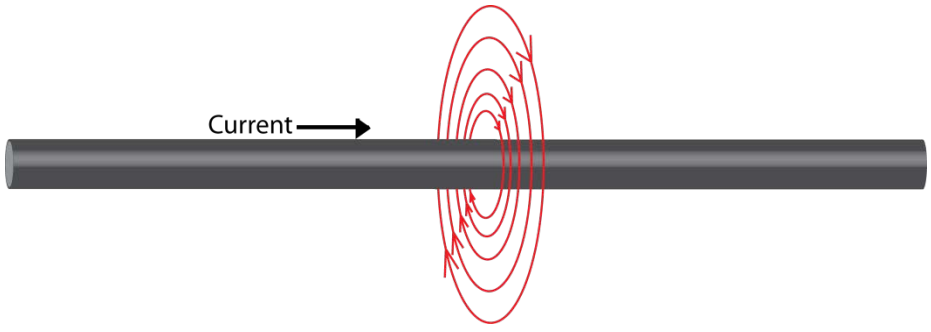

Figure 4-1: Magnetic field pattern created by a long wire. The field curves around the wire following the right hand rule.

To simplify construction, the two wire experimental setup is used in all of the following experiments; when only a single wire is needed, the second wire is simply removed to a distance where its effects are negligible.

The wires are driven to about 0.25 A by connecting them in parallel in the drain of a power MOS amplifier. The wires are modeled as a 1 ohm resistor as seen in Figure 4-2. The input voltage to the amplifier is a function generator. The current through the wires is found by probing the voltage across the 3.6 ohm source resistor. Using Ohm's law, the current in the source is found. The current in the drain (I_D) should be identical to that of the source (I_S). When a 4 V input signal is applied, the voltage across the resistor is about 2 V. The current in the source (and therefore the drain) is about 0.5 A. The long wires are assumed to have equal resistance, so the 0.5 A should be split between the two, about 0.25 A in each. Knowing the current, *I*, gives the magnetic field created a distance *r* from the wire with Ampere's law [25],

$$H = \frac{I}{2\pi r}. \tag{4-1}$$

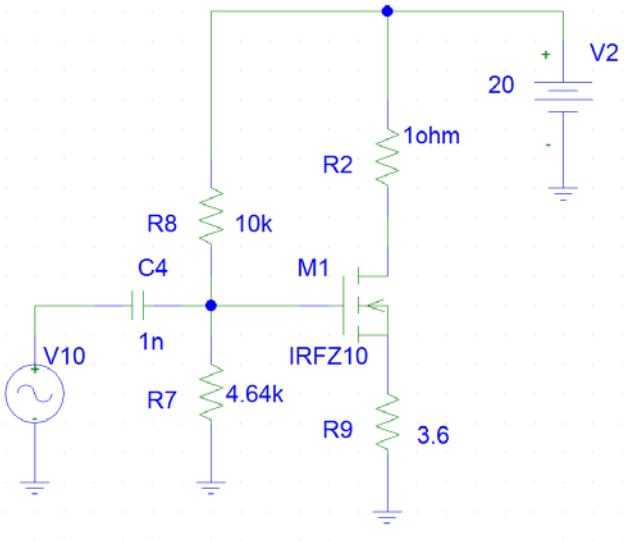

Figure 4-2: MOS amplifier setup used to drive a long wire to high current. The long wire is modeled as a 1 ohm resistor (in the drain).

4.2 SCOS Signal Measurement

Detecting high frequency magnetic fields with the sensor requires monitoring the change in transmitted power at a mid-resonant wavelength. A tunable laser tuned to a mid-resonant wavelength is used as input to the sensor. The mid-resonant wavelength at which the largest slope is centered is 1562 nm for the sensor used. The normalized spectrum of the sensor (shown in Figure 3-3) is included again for convenience in Figure 4-3. When a magnetic field causes a shift of $\Delta\lambda$ in the transmission spectrum, the output at this wavelength is modulated by ΔT. The transmitted power from the SCOS is received by an optical receiver to convert it into an electrical signal which is then read by a spectrum analyzer in order to discern the frequency content and signal strength of magnetic fields incident on the SCOS. The spectrum analyzer is set to a rolling average of 20 samples to increase signal to noise ratio. Figure 4-4 shows the system level view of the detection setup and includes a diagram of the SCOS transmission at a mid-resonance wavelength.

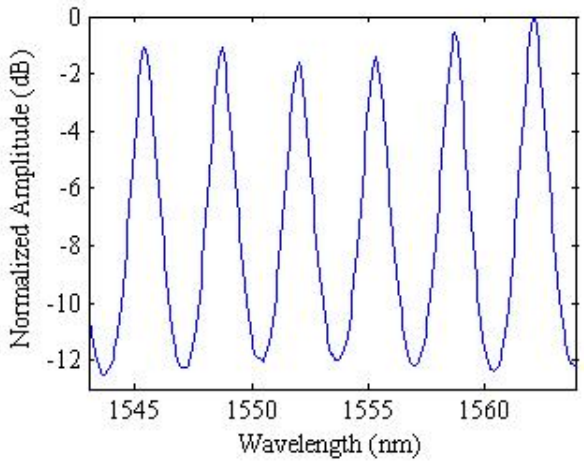

Figure 4-3: Transmission spectrum for a Bi-RIG MO-SCOS device with normalized amplitude. The resonant dips are about 10 dB.

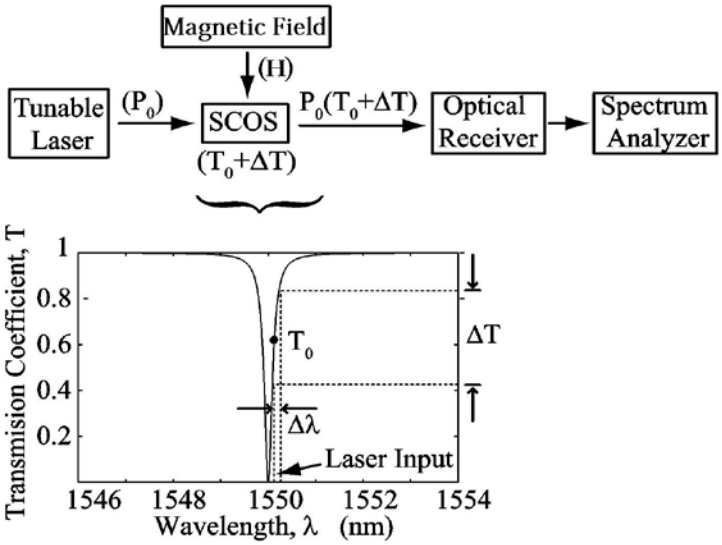

Figure 4-4: SCOS measurement setup system (Top). Diagram of SCOS transmission function (Bottom).

The signal received by the optical receiver is governed by the transmission function of the SCOS device, illustrated in Figure 4-4, and given by,

$$T = T_0 + \Delta T. \tag{4-2}$$

T_0 relates to the portion of the transmitted signal acting as the bias point, or DC component and ΔT represents the modulation signal at that bias point given by

$$\Delta T = \left(\frac{\Delta T}{\Delta \lambda}\right)\left(\frac{\Delta \lambda}{H}\right) H, \tag{4-3}$$

where the first term in parentheses is the slope of the transmission function and the second term in parentheses represents the spectral shift of the mode resonance due to the magnetic field, H. In full, the transmission function of the SCOS becomes,

$$T = T_0 + \left(\frac{\Delta T}{\Delta \lambda}\right)\left(\frac{\Delta \lambda}{H}\right)H. \tag{4-4}$$

With a bias power of P_o, the transmitted power from the SCOS at a biased wavelength into the optical receiver is

$$P_{in} = P_0 T_0 + P_0\left(\frac{\Delta T}{\Delta \lambda}\right)\left(\frac{\Delta \lambda}{H}\right)H, \tag{4-5}$$

and the signal portion of the output at the optical receiver, P_s, becomes

$$P_s = P_0\left(\frac{\Delta T}{\Delta \lambda}\right)\left(\frac{\Delta \lambda}{H}\right)H, \tag{4-6}$$

showing that the signal power increases linearly by three factors: (1) the optical input power, (2) the slope of the SCOS resonance at the bias point and (3) the spectral shift of the mode resonance due to H. Unknown magnetic fields can be determined by Equation (4-6), but solving for exact values of H requires that P_o, P_s, $\Delta T/\Delta \lambda$ and $\Delta \lambda/H$ are all known. P_o is user defined while P_s is measured. The spectrum slope $\Delta T/\Delta \lambda$ is dependent on the material's coupling strength. At this time, little will be said regarding the optimization of the $\Delta T/\Delta \lambda$ factor in MO sensors. Suffice it to say that for a material to couple well to the optical fiber it must have a very smooth surface and must also be thin (less than about 200 μm when working with a near IR source) to reduce coupling loss [4]. This slope factor can be solved in real time as demonstrated in 4.2.1. The $\Delta \lambda/H$ term is material dependent as well, and is addressed in Section 4.2.2.

4.2.1 Slope ($\Delta T/\Delta\lambda$)

A broadband ASE source is not ideal to determine the slope because it does not have a constant power output over its range of wavelengths. Instead, a tunable laser is used as the source. The tunable laser, which can be tuned in 1 pm steps, is tuned through a range of wavelengths, while the DC output power is read with an optical detector. This setup is controlled with Labview via GPIB serial bus, and produces a transmission versus wavelength as shown previously in Figure 3-3.

After the initial SCOS spectrum is measured as described above, the setup is made more user friendly by incorporating a "best slope" function into the Labview program. This makes SCOS measurement simpler by incorporating a Matlab script into the Labview program. This allows for a scan and analysis of the spectrum all in one simple GUI. An example spectrum is shown below in Figure 4-5. After obtaining this plot, the software found the best slope to be located at 1534.4 nm.

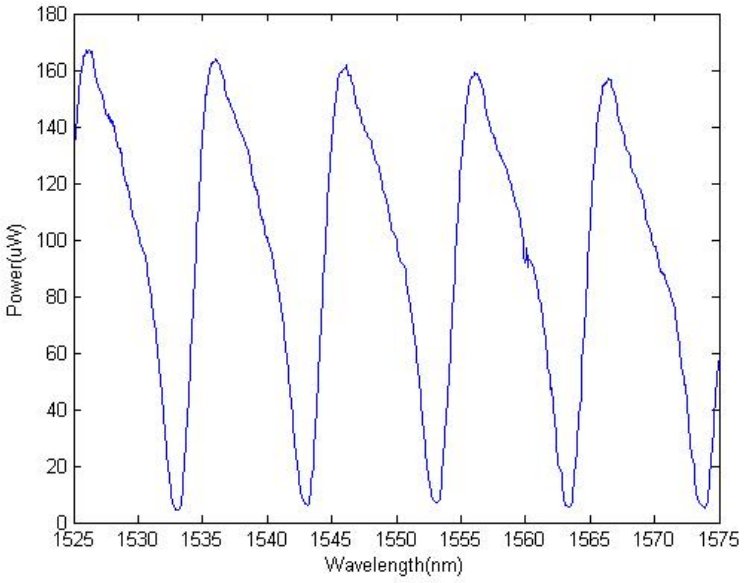

Figure 4-5: This sample SCOS spectrum (an EO SCOS) is analyzed for the best slope. The best slope found correctly attributed to be at 1534.4 nm.

The SCOS spectrum then incorporates in-situ slope monitoring. This is done by taking the best slope solved above, and repeatedly monitoring the DC power out at wavelengths immediately surrounding the area in question. The slope surrounding this area is monitored over time to account for slope variation caused by external factors such as temperature or strain. Thus, when a device is taken on-site, the different environmental conditions can be accounted for in real time.

4.2.2 Mode Shift ($\Delta\lambda/H$)

It has been shown that the Verdet constant directly affects the change in refractive index as a function of magnetic field $\Delta n/H$, which is correlated to $\Delta\lambda/H$. Unfortunately, the exact value for $\Delta\lambda/H$ cannot be solved with Equation (2-1) using the given information because the index, n_o, of the Bi-RIG sample has not been divulged by our supplier. But, one can solve for $\Delta\lambda/H$ in Equation (3-6) using a known field strength. The MO SCOS is placed 1 mm from the long wire described in the setup of Section 4.1 (and illustrated in Figure 4-6). The magnetic field in this setup is 43 A/m. As the input laser is swept through a small window of wavelengths as described in Section 4.2.1, the DC power out is found. This is done for several thousand samples and the average slope around the wavelength of interest is found. The signal power is measured by averaging 100 samples on the spectrum analyzer. Solving for $\Delta\lambda/H$ yields $2.65 \times 10^{-13} m^2/A$. Using this value of $\Delta\lambda/H$, an unknown field strength can be determined by measuring slope, optical input power, and signal power.

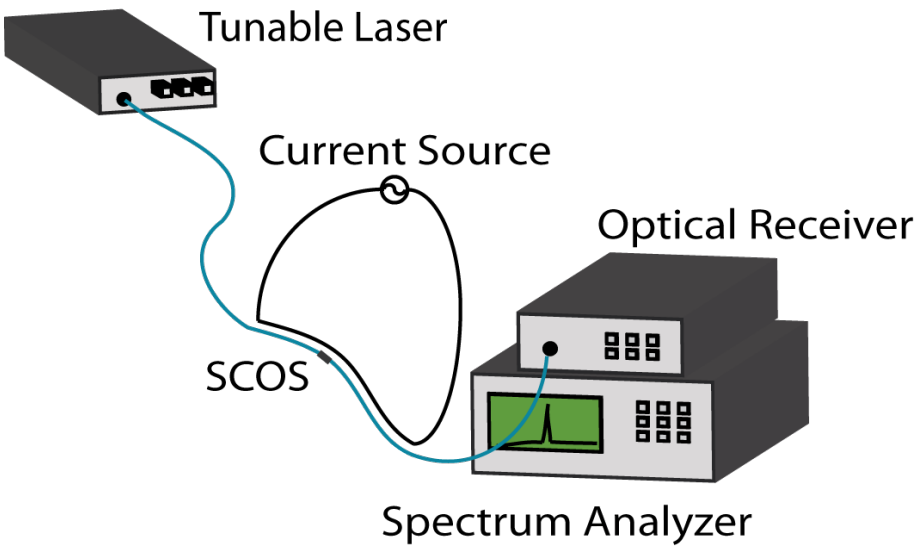

Figure 4-6: The MO SCOS detection setup. It utilizes a long current-carrying wire as the magnetic field source and a tunable laser as the optical source.

4.3 Minimum Detectable Field

Following the test setup described in Section 4.1 the sensor is initially placed 1 mm from a wire. This wire, carrying 0.27 A at 80 kHz creates a magnetic field of 43 A/m where the sensor is located. The second wire is several inches away, creating a negligible magnetic field at the sensor. Using the signal measurement technique described in Section 4.2, the SCOS signal was acquired with a spectrum analyzer. Figure 4-7 shows the output of the spectrum analyzer at the current field intensity. The magnetic field oscillates at 80 kHz; therefore, a peak signal at 80 kHz is shown. This peak is about 50 dB above the noise floor. At this point, the MO-SCOS sensor is removed from the proximity of both wires, and no signal is observed. This implies that the peak signal comes as a result of MO SCOS detection of the magnetic field and not some spurious source or pick-up.

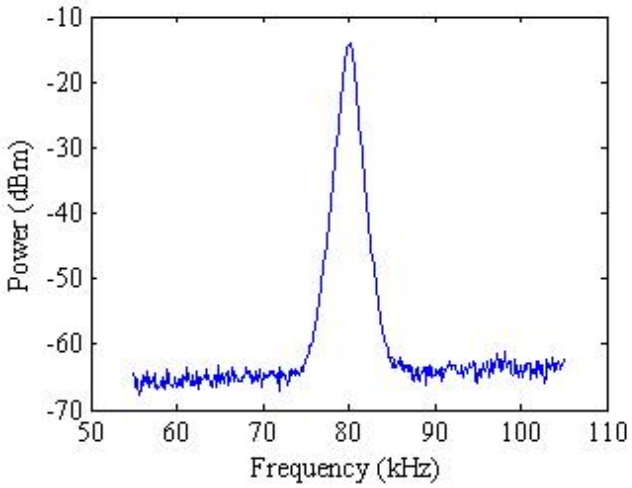

Figure 4-7: RF/Microwave Spectrum Analyzer measurements for Bi-RIG MO SCOS in a 43 A/m field.

The voltage driving the system is reduced until the signal is almost lost in the noise. This occurs when the current in each wire is 13.3 mA and the corresponding field-strength is 2 A/m. Figure 4-8 shows the signal measured in the 2 A/m field. The peak signal at 80 kHz is still about 2 dB above the average noise level. In this experimental setup, the MO SCOS sensor is able to accurately distinguish signal from noise at field strengths as low as 2 A/m.

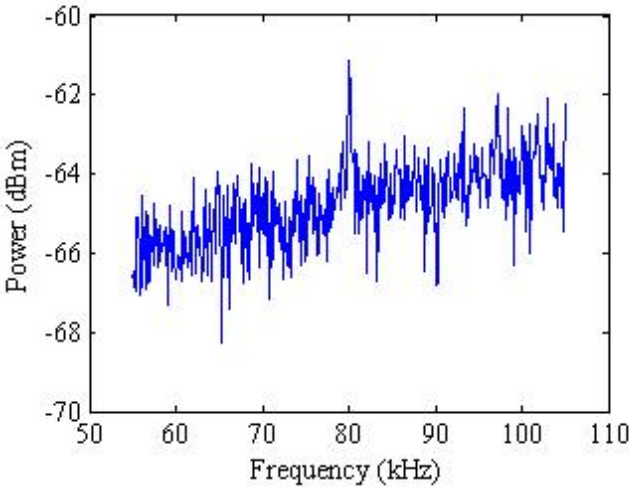

Figure 4-8: RF/Microwave Spectrum Analyzer measurements for Bi-RIG MO SCOS in a 2 A/m field

4.4 Spatial Localization

The small size of the MO SCOS lends itself well to field intensity localization. The MO effects take place only in the slab waveguide itself, which is less than 1 mm long (along the length of the fiber). This 1 mm length, the interaction length, should allow for a spatial resolution of 1 mm. The resolution can be demonstrated as a sensor is placed in the experimental setup described in Section 4.1. Again, the SCOS is driven with a tunable laser, and placed in close proximity to one long wire. The field generated (given by Equation (4-1)) should have a $1/r$ degradation as the sensor is moved away from the wire. The magnetic field in this arrangement is first simulated, and then compared to the actual measurements.

4.4.1 Simulated Field Pattern

The sensor can never be at zero distance from the wire, so this analysis is done as function of distance away from the wire in a plane 1 mm beneath it as demonstrated in Figure 4-9. A simulation of this configuration is done at a spatial resolution of 1 mm and 10 mm. As can be seen in Figure 4-10, the 10 mm resolution measurement convolves the field with a 10 mm long sensor, making the peak less defined.

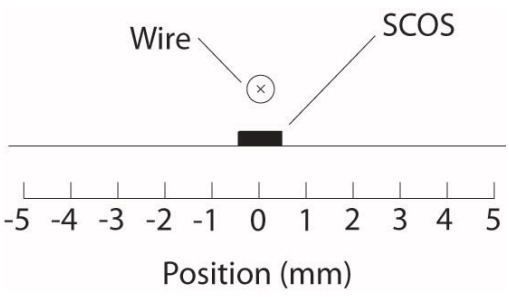

Figure 4-9: To measure the spatial sensitivity of the MO SCOS sensor, the sensor measures field intensity every 1 mm in a plane 1 mm from a wire. A cross section of the wire is represented by the circle, with the current flowing into the page.

This analysis is also performed with two wires. The wires are now 1 inch apart. A sensor with 1 mm resolution moved in a plane 1 mm from the parallel wires should look like the top plot in Figure 4-12. A spatial resolution of 10 mm is simulated in the bottom plot in Figure 4-12. Again, the peaks are less pronounced in this case.

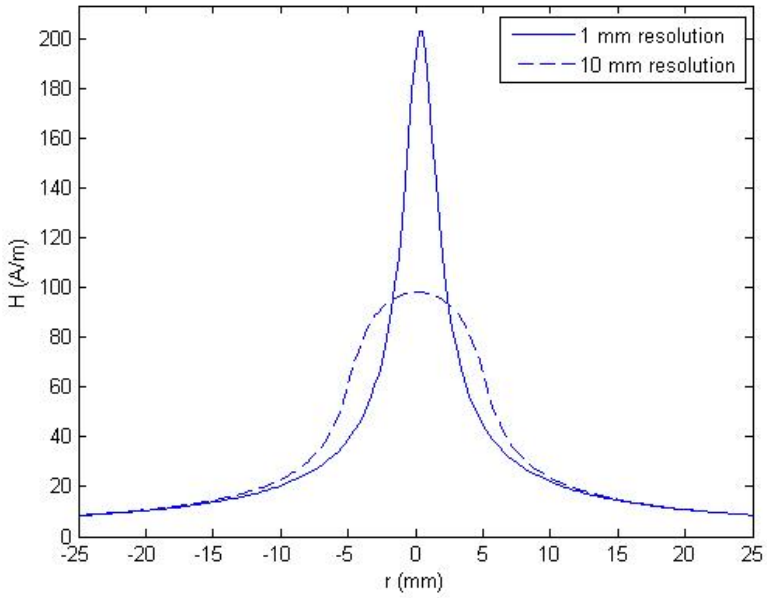

Figure 4-10: Simulated H-field as a function of distance from a long wire. The wire is located at r = 0 and the field pattern is analyzed in a plane 1 mm below the wire (where the sensor would be located). The simulation is done with both a 1 mm and 10 mm resolution.

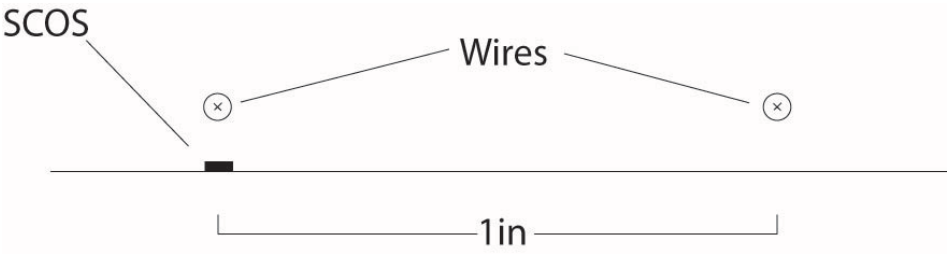

Figure 4-11: The spatial sensitivity of the MO SCOS if further analyzed by adding the second wire. The sensor measures field intensity every 1 mm in a plane 1 mm from the wires. A cross section of the wires is represented by the circles, with the current flowing into the page.

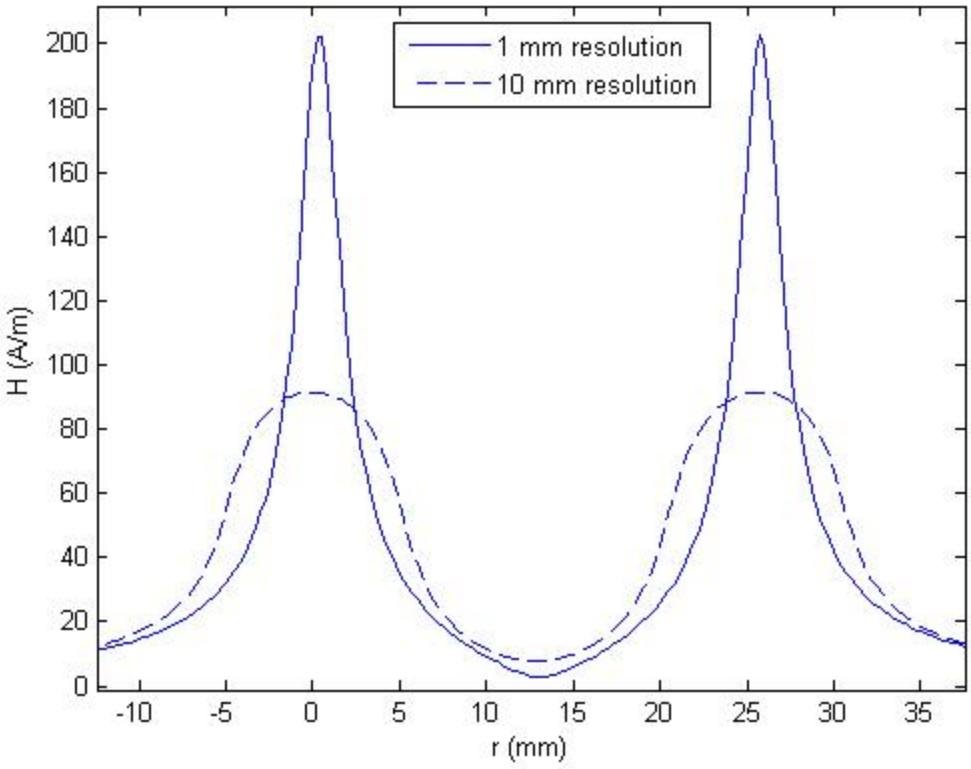

Figure 4-12: Simulated H-field as a function of distance from two long wires. The wires are 1 inch apart and located in a plane 1 mm above the sensor.

4.4.2 Actual Field Pattern

The simulations above are now realized experimentally. First, the sensor is placed in a plane 1 mm below the single wire. It is moved in 1 mm increments over a span of about 50 mm, passing directly under the wire in the center of the span. While the wire is driven with 0.27 A at 80 kHz, the spectral content through the SCOS is collected by the spectrum analyzer at each location. The signal power at 80 kHz at each position correlates directly with the field intensity (like Figure 4-7 and Figure 4-8 demonstrate). The peak signal versus position is converted to a

linear scale and plotted in Figure 4-13. The actual field measured follows the 1 mm resolution simulation in Figure 4-10. The peak is not wide and short like the 10 mm example.

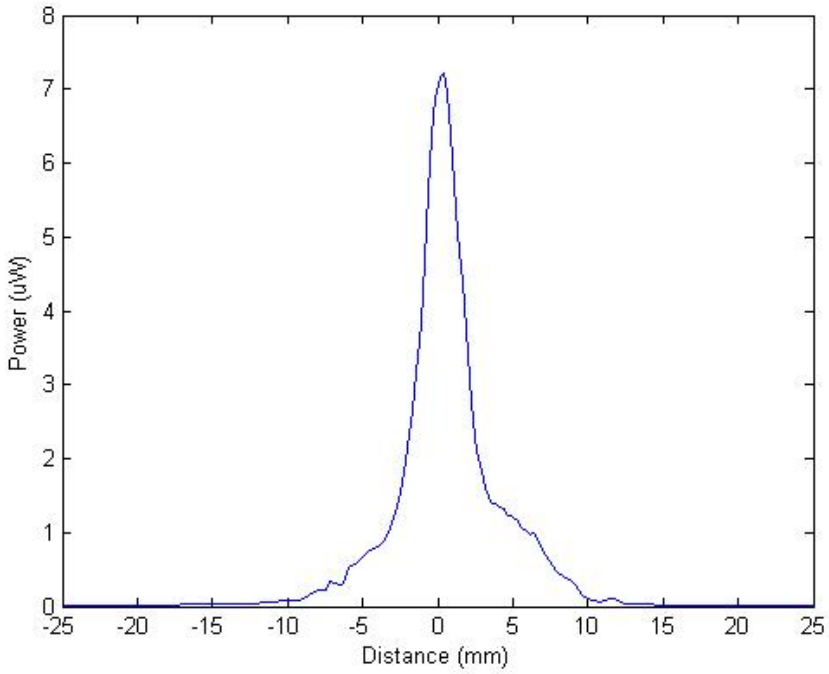

Figure 4-13: The spatial sensitivity of the MO SCOS sensor. The center (0 mm) corresponds to the location where the wire is directly above the sensor (1 mm above).

Next, an experiment is set up just as the second simulation described. The sensor is moved in a plane 1 mm below two parallel wires (as shown in Figure 4-11). This experiment also demonstrates a good spatial resolution with the abrupt peaks seen in Figure 4-14. These results differ, however, from the simulation. The two peaks here are not the same intensity. That is attributed to imperfections in the experimental setup. The two wires are likely not exactly 1 mm from the plane in which the sensor is moving. In this case, the field at the sensor would be stronger directly under a wire that is slightly closer than the other. It could also be attributed to soldering imperfections. If one wire has higher resistance due to poor soldering, it would have lower current, and thus a smaller field.

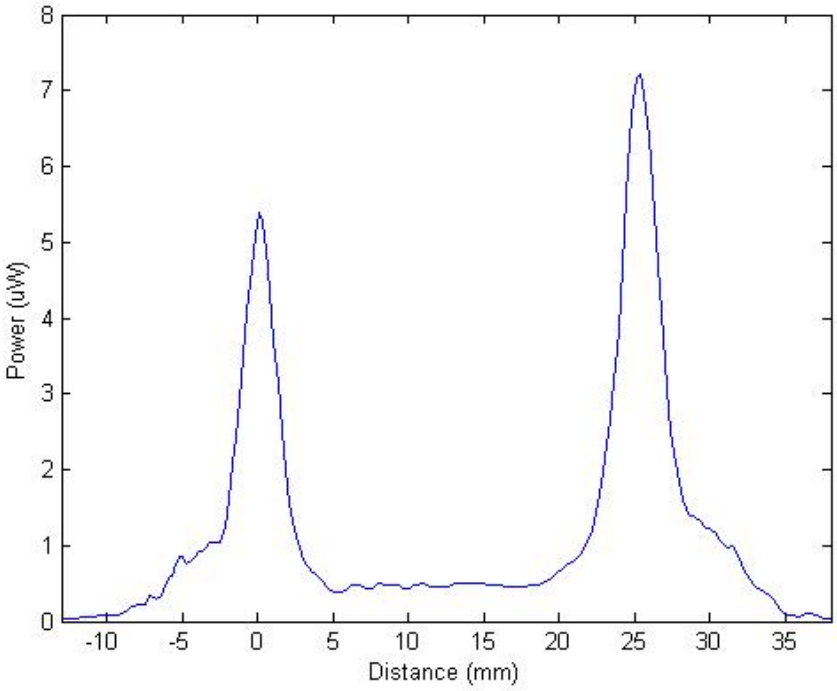

Figure 4-14: The spatial sensitivity of the MO SCOS sensor using two wires. The wires are directly above the sensor at 0 mm and 25.4 mm (1 inch).

5 ELECTRO-OPTIC SENSOR CONTRIBUTIONS

The main focus of this work has been in the creation of the magneto-optic slab coupled optical sensor. Some advancement has also been made implementing the electro-optic (EO) SCOS device. The EO sensor works much in the same way as the MO sensor. Incident electric field modulates the mid-resonant wavelength, which is measured as an AC signal power. This chapter explains efforts towards the implementation of the EO SCOS into a multi-dimensional measurement environment, an electromagnetic propulsion system, and a lower cost measurement solution.

5.1 Multi-axis Sensing

One of the benefits of the SCOS is the potential for multi-axial sensing. Vectorial measurements of electric fields have been demonstrated using free space coupling with bulk crystals [26, 27]. Additionally, fiber optic based sensors have also been proposed for mapping electric fields [28, 29]. SCOS technology makes 3-vector analysis of an electric field possible while adding the convenience of in-fiber technology. With SCOS technology, a multi-axial E-field sensor can be situated within a device to measure its fields while the light used to probe EO induced behaviors is fed through optical fiber. In this way multi-axial field measurements are possible and the portability of the sensor and measurement system is greatly improved over bulk optic counterparts requiring free-space coupling.

One version of a multi-axial SCOS sensor is implemented by placing three individual SCOS at orthogonal orientations on a probe as shown in Figure 5-1. With this multi-axial sensor configuration, each individual SCOS is fabricated to measure field strengths along the axis normal to its slab waveguide. Care must still be taken to ensure proper placement of each individual SCOS on the final probe to ensure orthogonal relations exist between the three individual sensors. With this setup, each SCOS in the spatially oriented multi-axial sensor is probed individually to acquire field strength measurements for its respective field orientation. The convenience of mounting sensors to the probe is countered by the increased size of the final sensor. In addition, each SCOS requires its own tunable laser, optical receiver and spectrum analyzer.

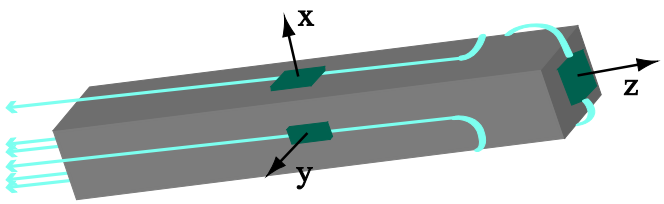

Figure 5-1: Diagram for a spatially aligned multi-axial sensor. Each SCOS sensor on the probe measures an independent axial direction.

Avoiding cross-axis sensitivity between orthogonal fields is a key concern in choosing an appropriate slab material for the compact multi-axial sensor. An EO polymer, which has high direction-dependent sensitivity [18], is the material of choice for compact multi-axial sensors. In the polymer, only a field aligned with the optic axis will produce alterations to its indices. The mixed axis terms, r_{42} and r_{51}, in the lower half of the EO tensor relate to the rotation of the

dielectric tensor from the presence of E_x and E_y fields [30]. However, due to the relatively large birefringence of polymer, even a large field of 10 MV/m (higher than the dielectric strength of air) in either the *x* or *y* direction rotates the dielectric tensor by less than one degree [30].

A two-dimensional EO SCOS has been fabricated after the manner shown in Figure 5-1 (but lacking the third, z, direction) and tested in a rotation stage. The rotation stage simply rotates the device in the middle of a pair of fixed electrodes. The electrodes produce the AC field while a tunable laser, optical detector, and spectrum analyzer are used as explained in Section 4.2. The graph in Figure 5-2 shows the normalized sensitivity of each SCOS acquired by the spectrum analyzer as a function of rotation angle. The measured signal for each sensor is strongest when the field is normal to that sensor. There is extinction greater than 400% as the field is perpendicular to each sensor.

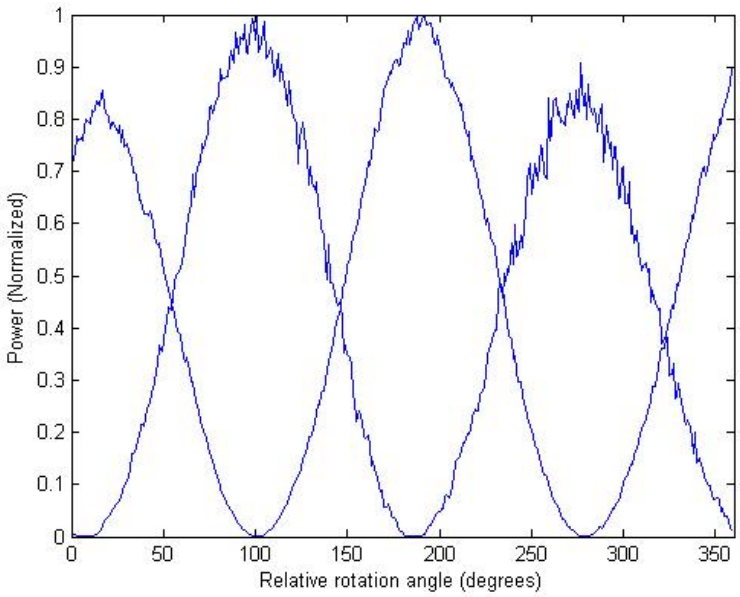

Figure 5-2: Dual-axis SCOS sensitivity as a function of rotation angle.

5.2 Electromagnetic Propulsion System

An electromagnetic rail gun (EMRG) launches a projectile with a large electric field rather than the conventional combustion reaction used in guns. This is done as current passes in opposite direction along two parallel conductive rails and creates a force down the center of the barrel [31]. The extreme field strengths and temperatures in the EMRG cause intense damage to the launchers, preventing them from consistent repeatable use [32]. Effort is currently focused on characterizing the large fields that exist between the rails to improve rail gun design. The EO SCOS device has been incorporated into several test launches as a potential method for characterizing the electric field.

The rail gun under test consists of two copper rails that are separated by epoxy-glass insulators while leaving a gap in the middle as shown in Figure 5-3. This whole rail and insulator setup is encased in a large confine to limit vibrations as photographed in Figure 5-4. To measure fields close to the rails, the EO sensor must be embedded in the T-shaped insulator and threaded through small exit holes placed in the metal encasing.

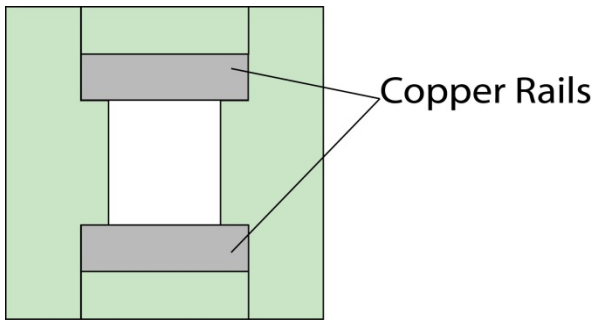

Figure 5-3: Cross-section diagram of rail gun rails and insulators. The hole in the center is where the projectile launches.

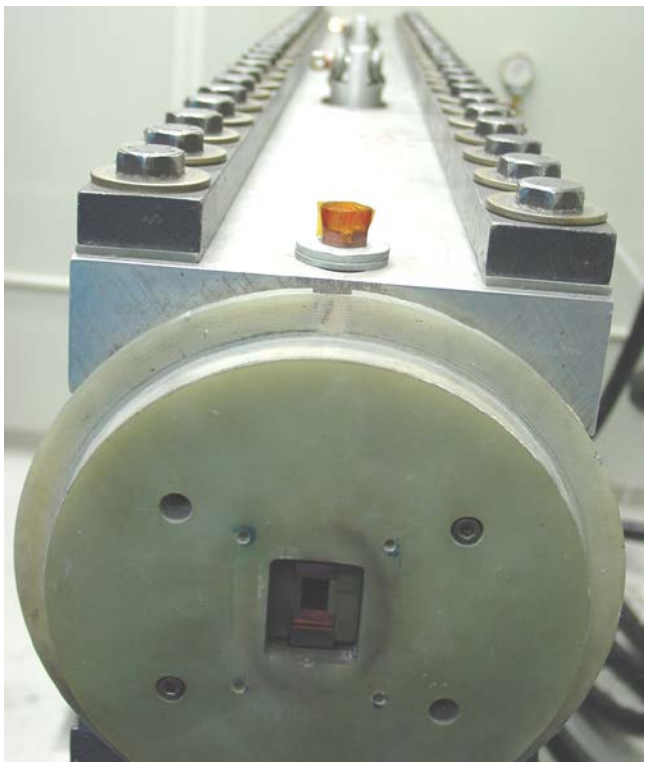

Figure 5-4: The large rail gun enclosure system used to limit vibrations. The small hole in the center is where the projectile launches and the copper rails can be seen above and below the hole.

Several mounting locations and techniques have been used over the series of tests performed with the rail gun. By following the sensor packaging convention outline in Section 3.2, the sensor is more sensitive to fields normal to the surface of the slab (as demonstrated in Section 5.1). The fields in different directions can be measured by fixing the sensors in different positions. The strongest field component will be normal to examples (*a)* and (*c)* in Figure 5-5 while sensors (*b)* and (*d)* are more sensitive to the perpendicular component of the field. The sensors are placed by milling rectangular holes out of the insulator. Sensors have been secured in place with a variety of epoxies as well as other means. Vibrations are a big issue, so the most successful means of mounting have been non-permanent. Vibrations have been minimized when

Cotton is used to cushion the sensor. The non-permanent mounting technique also helps with fiber input and output. Special care must be taken when threading the fiber into and out of the insulator. The large metal encasing has small exit points approximately every two inches that fit little more than an optical fiber. A permanent epoxy requires precise measurement to line the fibers up with the exit points, while a nonpermanent solution allows more freedom of movement.

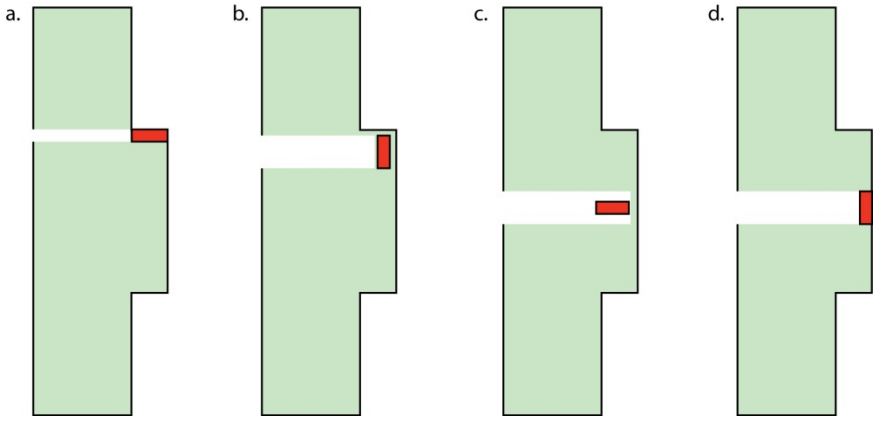

Figure 5-5: Sensors (in red) have been placed in the corner very close to the rail (a and b) and in the center in of the two rails (c and d). Figures a and c are in normal configuration while b and d are in transverse.

5.3 Portable SCOS Characterization

For the SCOS sensor to be cost efficient, we cannot expect the customer to obtain a spectrum analyzer to measure the SCOS signal, especially if SCOS arrays are implemented. Rather, a cheaper, more portable approach is being taken, using an oscilloscope. In keeping with this goal of portable SCOS signal measurement, effort has also been made to make SCOS spectrum characterization more affordable and portable. The current method of characterizing the SCOS spectrum is done by tuning through a range of wavelengths with a Santec tunable laser, while detecting the signal with a Newport optical detector. This is all controlled with

Labview via GPIB. A less expensive approach is as follows (see Figure 5-6 for block diagram): A Santur discrete tunable laser is the input to the sensor. It can be driven through an approximate range of wavelengths from 1530 to 1570 nm (in about 0.2 nm increments). The power out of the sensor is detected by a Thor InGaAs detector. The current out of the detector is linearly proportional to the power in, so a load resistor and oscilloscope can be used to measure the DC signal. These components are cheaper than the alternative method. Also, the laser source and oscilloscope can be controlled with Labview via USB rather than GPIB. To make the setup even more accessible, the Labview program can be exported as an executable for use on PCs without Labview. The in-situ slope monitoring explained in Section 4.2.1 has also been incorporated into the new setup.

Figure 5-6: Block diagram for portable SCOS spectrum measurement.

6 CONCLUSION

The magneto-optic slab coupled optical sensor (MO SCOS) provides a good magnetic field sensing option. Their in-fiber design makes them small and easy to integrate into even large and complex systems. This MO sensor can detect magnetic fields down to 2 A/m with a 1 mm spatial resolution.

6.1 Contributions

As mentioned in the introduction, the main contributions in this work have been in the development of the magneto-optic SCOS. A small amount of work has been also done in advancing the electro-optic SCOS. All the contributions in this work are outlined as follows:

- I designed a magneto-optic sensor based on coupling of light between a D-fiber and a slab of Bi-RIG (a magneto-optic material). The technique is called MO-SCOS.
- I developed the techniques to fabricate the MO-SCOS.
- I characterized the MO-SCOS performance in terms of:
    - Signal strength
    - Field sensitivity
    - Spatial localization
- I integrated Electro-optic sensors into an electromagnetic rail gun.

- I have been involved in EO sensor research with several of my peers, including the multi-dimensional EO sensor.

6.1.1 MO-SCOS Development

This work outlines the theory of the magneto-optic slab coupled fiber optic sensor. The good coupling and large Verdet constant of bismuth-doped rare earth iron garnet make it the material of choice. Mode coupling between D-fiber and the Bi-RIG waveguide make this sensor possible. As an AC magnetic field is applied to the slab, the allowable modes of light traveling through the sensor have a resulting shift in wavelength. This $\Delta\lambda$ can be utilized to create an AC change in power, which is recognized by a spectrum analyzer.

6.1.2 MO-SCOS Fabrication

The magneto-optic material bismuth-doped rare earth iron garnet (Bi-RIG) is used as the slab waveguide for the SCOS sensor. In-situ monitoring during the slab placement ensures good mode coupling, which is necessary to increase sensitivity. The sensor is also packaged into a protective substrate to protect from breaks and contamination.

6.1.3 MO-SCOS Characterization

The MO sensor has been incorporated into a variety of tests. The minimum detectable field is found to be 2 A/m and the spatial resolution of the sensor is demonstrated to be 1 mm. The slope of the sensor can be monitored in real time, and the shift has been solved to be 2.65 x

10^{-13} m^2/A. Using the slope and the shift, an unknown magnetic field can be found with this MO sensor.

6.1.4 EO-SCOS Implementation in EMRG

The electro-optic sensors have been implemented into the insulation of an electromagnetic rail gun. Some real challenges have been overcome in order to get the fragile fiber optic sensors threaded into a rail gun and embedded inside.

6.1.5 Multi-axis EO SCOS Development, Presentation, and Publication

This work has also furthered the development of the EO SCOS by experimenting with a two-dimensional sensor. The sensor, which would require two sources and detectors, experiences over 10 dB of extinction from on-axis to off-axis measured field. The multi-axis SCOS results and the overall SCOS development were collected and presented at a professional conference and will be published in a peer reviewed journal, the *Journal of Directed Energy*.

6.2 Future Work

This study has by no means attempted to be an exhaustive study of the theory, fabrication, and application of the SCOS sensor. Much can be done in the future to fortify the principles that have now been established.

6.2.1 MO Materials

The MO SCOS efforts were concentrated solely on bismuth-doped rare earth iron garnet. A more thorough study of other MO materials and the implications their properties would have on SCOS development could be beneficial.

Also, this work has not made an effort to understand the directional dependence of the MO sensor. Bi-RIG and other MO materials could be studied to search for materials that would be more sensitive to the direction of incidence of the H-field. More directionally sensitive sensors could be used in multi-axis field mapping.

6.2.2 System Interrogation

Much effort needs to still be done to interrogate SCOS sensors into more useful environments. As of now, the SCOS device can only detect AC fields. Work can be done in the area of electromagnetic pulse sensors.

Work can also be done to improve the data acquisition. Although the sensor is monitored in real time, the Spectrum Analyzer takes time to acquire each sample, so the number samples per second is low. The sensor could benefit by utilizing an oscilloscope in its place.

It is also known that temperature and strain affect the SCOS behavior. Effort can be made in the area of sensor hardening.

REFERENCES

1. Kim, K., et al., *Polarizing properties of optical coupler composed of single mode side-polished fiber and multimode metal-clad planar waveguide.* Optics Communications, 2000. **180**: p. 37-42.

2. Sohn, K. and J. Song, *Thermooptically tunable side-polished fiber comb filter and its application.* IEEE Photonics Technology Letters, 2002. **14**: p. 1575-1577.

3. Jung, W., et al., *High-sensitivity temperature sensor using a side-polished single-mode fiber covered with the polymer planar waveguide.* IEEE Photonics Technology Letters, 2001. **13**: p. 1209-1211.

4. Gibson, R., et al., *Electro-optic sensor from high Q resonance between optical D-fiber and slab waveguide.* Applied Optics, 2008. **47**(13).

5. Gibson, R., et al., *Improved sensing performance of D-fiber/planar waveguide couplers.* Optics Express, 2007. **15**(5).

6. Gibson, R., *Slab Coupled Optical Fiber Sensors for Electric Field Sensing Applications*. 2009: Brigham Young University.

7. Pevler, A.E. *Security implications of high-power microwave technology*. in *Proceedings of the 1997 International Symposium on Technology and Society*. 1997. Piscataway, NJ, USA: IEEE.

8. Van Keuren, E. and J. Knighten. *Implications of the high-power microwave weapon threat in electronic system design*. in *1991 IEEE International Symposium on Electromagnetic Compatibility*. 1991. Piscataway, NJ, USA: Publ by IEEE.

9. Miller, C.R., *Electromagnetic Pulse Threats in 2010*. 2005: United States. p. 29.

10. Foster, J.J., et al., *Report of the Commission to Assess the Threat to the United States from Electromagnetic Pulse (EMP) Attack. Volume 1: Executive Report*. 2004: United States. p. 62.

11. Corp., B.K.P. (2011) *Handheld Spectrum Analyzers, 3.3 GHz & 8.5 GHz Models 2650A, 2652A, 2658A*.

12. Technologies, P. *Magnetic Field Sensor (B) Model B-100*. 2009; Available from: http://prodyntech.com/home/page/model_b_1__.

13. Sze, S.M. and K.N. Kwok, *Physics of Semiconductor Devices*. 2007: John Wiley & Sons Inc.

14. Shirasaki, M., *Faraday rotator assembly*. 1986, Fujitsu Limited: Japan.

15. Heredero, R., et al., *Micromachined optical fiber current sensor.* Applied Optics, 1999. **38**(25): p. 5298-5305.

16. Itoh, N., et al., *Small optical magnetic-field sensor that uses rare-earth iron garnet films based on the Faraday effect.* Applied Optics, 1999. **38**(10): p. 2047-2052.

17. Sun, L., S. Jiang, and J. Marciante, *All-fiber magnetic-field sensor based on Faraday rotation in highly terbium-doped fiber.* Optics Express, 2010. **18**(6): p. 5407-5412.

18. Gibson, R., R. Selfridge, and S. Schultz, *Electric field sensor array from cavity resonance between optical d-fiber and multiple slab waveguides.* Applied Optics, 2009. **48**(19): p. 3695-3701.

19. Kim, K.T., D.S. Yoon, and G.-I. Kwoen, *Optical properties of side-polished polarization maintaining fiber coupled with a high index planar waveguide.* Optics Communications, 2004. **230**(1-3): p. 137-144.

20. Chandani, S.M. and N.A.F. Jaeger, *Fiber-optic temperature sensor using evanescent fields in D fibers.* IEEE Photonics Technology Letters, 2005. **17**(12): p. 2706-2708.

21. Gibson, R., et al., *Improved sensing performance of D-fiber/planar waveguide couplers.* Optics Express, 2007. **15**(5): p. 2139-2144.

22. Landau, L.D., et al., *Electrodynamics of Continuous Media*. 1960: Addison-Wesley Publishing Company, Inc.

23. Grumman, N. *TGG Data Sheet*. 2003; Available from: http://www.as.northropgrumman.com/products/synoptics_tgg/assets/tgg_data_sheet.pdf.

24. Brandle, C.D., V.J. Fratello, and S.J. Licht, *Magneto-optic material having low magnetic moment*. 1997, Lucent Technologies Inc.: USA. p. 5.

25. Ulaby, F., *Fundamentals of Applied Electromagnetics*. 5 ed. 2007, Upper Saddle River, NJ: Pearson.

26. Gaborit, G., J.L. Coutaz, and L. Duvillaret, *Vectorial electric field measurement using isotropic electro-optic crystals.* Applied Physics Letters, 2007. **90**(24): p. 241118.

27. Kuo, W.-K., Y.-T. Huang, and S.-L. Huang, *Three-dimensional electric-field vector measurement with an electro-optic sensing technique.* Optics Letters, 1999. **24**(22): p. 1546-1548.

28. Katehi, L.P.B., K. Yang, and J.F. Whitaker, *Electric field mapping system using an optical-fiber-based electrooptic probe.* IEEE Microwave and Wireless Components Letters, 2001. **11**(4): p. 164-166.

29. Wakana, S., et al., *Novel electromagnetic field probe using electro/magneto-optical crystals mounted on optical-fiber facets for microwave circuit diagnosis.* IEEE MTT-S International Microwave Symposium Digest, 2000. **3**: p. 1615-1618.

30. Yariv, A. and P. Yeh, *Photonics: Optical electronics in modern communications*, in *The Oxford series in electrical and computer engineering*. 2007, Oxford University Press: New York. p. 406-418.

31. Jensen, D.B., *Electromagnetic Rail Gun*. 1992, The United States of America as represented by the Secretary of the Air Force: United States.

32. Physorg.com (2004) *Smoothing Out Kinks in Electromagnetic Propulsion Will Bring Technology From Research to Practical Use*. PHYSorg.com.

APPENDIX A. H-FIELD FROM A LONG WIRE -SIMULATION CODE

This MATLAB code demonstrates the H-field intensity as a function of distance away from the wire. It was designed to mimic an actual measurement setup, where the sensor cannot have zero distance from the wire.

```
%%%%%%%%%%%%%%%%%%%%%%%%%%%%%%%%%%%%%%
%Bryson Shreeve
%
%Program created to determine H-field caused by long parallel wires.  When magneto-
%optic sensor is placed near the wires, it will experience this magnetic field.  Sensor is
%orthogonal to the direction of the long, current-carrying wires.  As an electric current
%propagates through the wire, a magnetic field is created around the wire.
%%%%%%%%%%%%%%%%%%%%%%%%%%%%%%%%%%%%%%

clear all;
close all;

I =.25;                     %A
u_o = 4*pi*10^-7;           %T*m/A
y = .001;                   %initial y distance (m)
d_in = 1;                   %distance between the two wires (in)
d = d_in*0.0254;            %meters


%%Part 1 %%%%%%%%%%%%%%%%%%%%%%%%%%%%%%%%
%H as a function of distance away from one long wire

x = (-35:.25:35)/1000;      %meters  -in .25 mm increments
r = sqrt(x.^2+y^2);         %meters
H = I./(2.*pi.*r);          %A/m

plot(x*1000,H);hold;
plot(0,0:200);
title('H-field as a function of distance from a long wire');
xlabel('r (mm)');
```

```
ylabel('H (A/m)');
axis([-d*1000 d*1000 0 max(H)+10]);

%%Part 1a %%%%%%%%%%%%%%%
%Convolve with 1mm
H_1mm = conv(H,[1 1 1 1])/4;    %avg .5 mm to left and .5mm to right
figure;
plot(x*1000,H_1mm(1:length(H)-0));hold;
%title('H-field as a function of distance from a long wire');
xlabel('r (mm)');
ylabel('H (A/m)');
axis([-25 25 0 max(H_1mm)+10]);

%%Part 1b %%%%%%%%%%%%%%%
%Convolve with 10mm
H_10mm = conv(H,ones(1,40))/40;    %avg 10 mm to left and 10mm to right
plot(x*1000,H_10mm(20:length(H_10mm)-20),'--b');
%title('H-field as a function of distance from a long wire');
xlabel('r (mm)');
ylabel('H (A/m)');
legend('1 mm resolution','10 mm resolution')


%%Part 2 %%%%%%%%%%%%%%%%%%%%%%%%%%%%%%%%%%%%%%%%%%%%%%%%%%%%%%%%%%%%%%%%
%H as a function of distance from 0 to d on a plane 1mm above two parallel
%wires.
x1 = (-20:.25:55)/1000; %m
x2 = x1-d;                %m
r1 = sqrt(x1.^2+y^2);       %m
r2 = sqrt(x2.^2+y^2);       %m
theta1 = asin(y./r1);       %rad
theta2 = asin(y./r2);       %rad

%Since MO SCOS isn't really directionally dependent, H can be broken down
%into x and y, and the Hx's and Hy's can be added together.
H1 = I./(2.*pi.*r1);
Hx1 = sin(theta1).*H1;
Hy1 = cos(theta1).*H1;
H2 = I./(2.*pi.*r2);
Hx2 = sin(theta2).*H2;
Hy2 = cos(theta2).*H2;

Hx = Hx1 + Hx2;
Hy = Hy1 - Hy2;
H = sqrt(Hx.^2 + Hy.^2);    %A/m
```

```
figure;
plot(x1*1000,H);hold on;
plot(0,0:250);
plot(d*1000,0:250);hold off;
title(strcat('H-field in a plane 2mm above two wires (of parallel current) separated by d=',
num2str(d*1000), 'mm'));
xlabel('r (mm)');
ylabel('H (A/m)');
axis([-(d*1000+1) (2*d*1000+1) 0 max(H)+10]);

%%Part 2a %%%%%%%%%%%%%%%
%Convolve with 1mm
H_1mm = conv(H,[1 1 1 1])/4;          %avg .5 mm to left and .5mm to right
figure;
plot(x1*1000,H_1mm(1:length(H)-0));hold;
%title('H-field as a function of distance from a long wire');
xlabel('r (mm)');
ylabel('H (A/m)');
axis([-25 25 0 max(H_1mm)+10]);

%%Part 2b %%%%%%%%%%%%%%%
%Convolve with 10mm
H_10mm = conv(H,ones(1,40))/40;    %avg 10 mm to left and 10mm to right
plot(x1*1000,H_10mm(20:length(H_10mm)-20),'--b');
%title('H-field as a function of distance from a long wire');
xlabel('r (mm)');
ylabel('H (A/m)');
legend('1 mm resolution','10 mm resolution')
```